Non-decoupled morphological evolution of the fore- and hind limb of sabretooth predators

Alberto Martín-Serra[1*†], Borja Figueirido[1], Paul Palmqvist[1]

[1]Departamento de Ecología y Geología, Facultad de Ciencias, Universidad de Málaga, Campus de Teatinos s/n, 29071-Málaga, Spain.

Short title: Limb integration in sabretooths

[*]To whom correspondence may be addressed. E-mail: almarse@uma.es

[†]Current address:

Department of Earth Sciences, University of Oxford

South Parks Road, Oxford, United Kingdom

OX1 3AN

Abstract

Specialized organisms are useful for exploring the combined effects of selection of functional traits and developmental constraints on patterns of phenotypic integration. Sabretooth predators are one of the most interesting examples of specialization among mammals. Their hypertrophied, sabre-shaped upper canines and their powerfully built forelimbs have been interpreted as adaptations to a highly specialized predatory behaviour. Given that the elongated and laterally compressed canines of sabretooths were more vulnerable to fracture than the shorter canines of conical-tooth cats, it has been long hypothesized that the heavily muscled forelimbs of sabretooths were used for immobilising prey before developing a quick and precise killing bite. However, the effect of this unique adaptation on the covariation between the fore- and the hind limb has not been explored in a quantitative fashion. In this paper, we investigate if the specialization of sabretooth predators decoupled the morphological variation of their forelimb with respect to their hind limb or, in contrast, both limbs vary in the same fashion as in conical-tooth cats, which do not show such extreme adaptations in their forelimb. We use three-dimensional geometric morphometrics and different morphological indices to compare the fore- and hind limb of conical- and sabretooth predators. Our results indicate that the limb bones of sabretooth predators covary following the same trend of conical-tooth cats. Therefore, we show that the predatory specialization of sabretooth predators did not result in a decoupling of the morphological evolution of their fore- and hind limbs. The role of developmental constraints and natural selection on this coordinate variation between the fore- and the hind limb is discussed in the light of this new evidence.

Keywords: Phenotypic integration, Specialization, Sabretooth carnivores, Forelimb, Hindlimb.

Introduction

Phenotypic integration and modularity are outcomes of the interplay between pleiotropy, developmental constraints, and functional adaptations (Wagner & Altenberg, 1996; Hallgrímsson et al. 2002; Young & Badayev, 2006; Wagner et al. 2007; Klingenberg, 2008; Hallgrímsson et al. 2009). Therefore, the characterization of integrated or modular patterns is crucial to understand how these factors shape phenotypic evolution. Within this context, organisms with highly specialized structures and behaviours are very useful to study the adaptive aspects of morphological evolution. This is because such specializations may imply overriding the constraints imposed by other factors (i.e., genetic or developmental) and may cause changes on the patterns of integration (Wagner & Altenberg, 1996; Young & Badayev, 2006; Wagner et al. 2007). For example, several authors have demonstrated changes in integration patterns due to dietary specializations (Monteiro & Nogueira, 2010), changes in reproductive strategies (Goswami et al. 2009; 2012) or differences in locomotor modes (Young & Hallgrímsson, 2005; Bell et al. 2011; Martín-Serra et al. 2015). Here, we test if the predatory specialization of sabretooth predators resulted also in a change in the pattern of covariation between the fore- and hind limb of these mammalian carnivores.

Among the living large carnivores, higher than expected frequencies of canine breakage are observed compared to other teeth (Van Valkenburgh and Hertel, 1993; Van Valkenburgh, 2009). This is most likely the result of injury during the killing of prey and carcass processing, because the length of the upper canines makes them most susceptible to tooth to bone contact and to the large, unpredictable bending loads generated when they are driven into mobile prey. For this reason, the elongated and

laterally compressed canines of sabretooths were more vulnerable to fracture than the stout, conical canines of modern felids. In order to minimize the risk of canine fracture, it has been long hypothesized that the heavily muscled forelimbs of sabretooths were imperative for pulling down and immobilising prey before positioning the bite over the prey throat or belly, where bite depth is essential to generate strikes reaching major blood vessels (Gonyea, 1976; Akersten, 1985; Anyonge, 1996; Antón et al. 2004; Christiansen, 2008; Salesa et al. 2010; Andersson et al., 2011; Meachen-Samuels, 2012), or even for delivering a non-biting stab with the jaw closed for inflicting a pneumothorax, which would even decrease more canine exposure to fracture (Wilson et al., 2013). In any case, the functional need of immobilising prey is reflected in the skeletal anatomy of the North American sabretooth cat *Smilodon fatalis,* in which the short and robust forelimb bones were reinforced by cortical thickening to a greater degree than in the extant pantherine cats, which allowed it to withstand the loadings generated by the struggles of prey while developing a quick and precise killing bite (Meachen-Samuels & Van Valkenburgh, 2010). In contrast, the living felids have conically shaped upper canines that they use to hold a prolonged bite in the muzzle or neck of their prey until it dies from suffocation. Therefore, in conical-tooth cats the role of the forelimbs while subduing prey is not as important as in the case of sabretooth predators (McHenry et al. 2007; Salesa et al. 2010; Meachen-Samuels, 2012).

Concerning the body proportions of sabretooths, Anyonge (1993) estimated the body mass of *S. fatalis* using two sets of regression equations based on a number of humeral and femoral measurements derived from a sample of living carnivores and from a sample of living felids, respectively. The mean mass estimated with the first set of equations was similar for those based on the humerus (355 kg) and the femur (347 kg). However, the mass estimates derived from the regressions based on felids were

systematically higher for the humerus (442 kg on average) than for the femur (369 kg) (Anyonge, 1993). This suggests that *S. fatalis* had more powerfully developed forelimbs than hind limbs compared to the extant conical-shaped cats, but similarly scaled fore- and hind limbs compared to other carnivores.

Given the arguments outlined above, many researchers have highlighted the extremely strong forelimbs of sabretooth forms in comparison with those of extant conical-tooth cats (Anyonge, 1996; Antón et al. 2004; Christiansen & Harris, 2005; Salesa et al. 2010; Meachen-Samuels & Van Valkenburgh, 2010; Lewis & Lague, 2010). However, less attention has been paid to the hind limbs of sabretooth predators (but see Meachen-Samuels & Van Valkenburgh (2010) and Lewis & Lague (2010)).

Previous researchers have demonstrated that quadrupedal placental mammals have a conserved integrated pattern between the fore- and the hind limb (Young & Hallgrímsson, 2005; Goswami et al. 2012; Martín-Serra et al. 2015). This has been associated with the developmental origin of both limbs, which are serially homologous (Young & Hallgrímsson, 2005; Goswami et al. 2012). This brings up questions on the evolutionary interplay between the effects of the adaptive process that shaped the forelimb of sabretooths and the constraints posed by the integrated developmental pattern between the fore- and hind limb that these predators inherited from their mammalian ancestor.

In this article, we examine if the specialization towards strong forelimbs in sabretooth forms led to a decoupled phenotypic pattern between their fore- and hind limbs. To do this, we first use 3D geometric morphometrics to quantify the morphological covariation (as a proxy for phenotypic integration) between limb bones in sabre- and conical-tooth forms. Then, we also compare several proxies for limb strength (i.e., resistance to stresses) to test if sabretooth predators have stronger

forelimbs than hind limbs relative to conical-tooth cats. We hypothesize that a strong effect of natural selection to shape such specialized predatory behaviour has decoupled the morphological evolution of the fore- and the hind limb in sabretooth carnivores in comparison with the living predatory mammals.

Materials and Methods

The dataset studied comprises 49 humeri, 60 radii, 49 ulnae, 51 femora, and 52 tibiae from 10 species of living felines (Felidae, Carnivora) and 10 extinct taxa belonging to the families Felidae, Barbourofelidae and Nimravidae (table 1). Living and extinct taxa were divided into two morphotypes according to their canine morphology: conical-tooth and sabretooth forms (figure 1*a*). Conical-tooth predators include all living felines (Martin, 1980; Slater & Van Valkenburgh, 2008) plus the extinct *Pseudaelurus* sp. (Biknevicius et al. 1996). All remaining extinct taxa are sabretooth predators (machairodontine felids, barbourofelids and nimravids according to (Slater & Van Valkenburgh, 2008). We included only limb bones from adult specimens (as indicated by the complete fusion of the epiphyses to the diaphysis) in our sample to avoid the effects of ontogenetic variation. Identity numbers and hosting institutions of all modern and fossil specimens are provided in tables S1 and S2.

We digitized a set of three-dimensional landmarks for each bone (figure 1*b*) with a Microscribe G2X and imported their (x,y,z) coordinates into a spreadsheet using the Immersion software package (Immersion, Inc., San Jose, CA, USA). Landmarks were chosen following different anatomical criteria (table S3) for capturing the most important aspects of their morphology. Although most landmarks were digitized on bone epiphyses, four midshaft landmarks were also digitized to capture the circumference of the diaphysis, because it is a very important biomechanical aspect in

limb motion and body weight support (Bertram & Biewener, 1990; Anyonge, 1993; 1996).

We scanned the bones of one individual of jaguar (*Panthera onca*, AMNH 139959) with a 3D-mobile surface scanner (Nextengine 3D and the software package ScanStudio Pro). The landmarks digitized were also located in these 3D models to visualize the hypothetical morphologies obtained from statistical analyses using the morphing procedure (Wiley et al. 2005; Drake & Klingenberg 2008; Singleton, 2012; Martín-Serra et al. 2014a; 2014b) of software Landmark (Institute of Data Analysis and Visualization, IDAV 2002–2006).

We performed a Procrustes fit (Dryden & Mardia, 1998) of all landmark coordinates of each bone separately, and we averaged these Procrustes coordinates by species. We also calculated the centroid size (Cs) of each bone as a proxy for bone size. All these procedures were performed using the software MorphoJ (Klingenberg, 2011).

We assembled a composite phylogenetic tree (figure 1*a*) using Mesquite (Maddison & Maddison, 2011) and following different published sources. In the case of extant taxa, we obtained the phylogenetic position and branch lengths from the molecular supertree of Nyakatura and Bininda-Emonds (2012). For the extinct taxa, branch lengths were estimated from the stratigraphic ranges provided by several sources, as well as from their phylogenetic position (for detailed information and references see table S4). Where estimates of branch lengths based on molecular data and on stratigraphic ranges differed, the oldest date was chosen. In those cases in which consecutive nodes overlapped at the same date, an arbitrary difference of 0.1 Myr was introduced.

This composite tree was imported into MorphoJ (Klingenberg, 2011) to perform the phylogenetic independent contrasts of Procrustes coordinates and Log-Cs to account for the phylogenetic signal in these variables.

To take into account the effects of evolutionary allometry, we performed a series of multivariate regressions (Monteiro, 1999) between the contrasted Procrustes coordinates and the contrasted Log-Cs for each bone (Figueirido et al. 2013). We applied this vector of evolutionary allometry to the original dataset of species averages to extract the residuals (i.e., morphological changes not explained by size differences following different authors (Klingenberg & Marugán-Lobón, 2013; Martín-Serra et al. 2014a; 2014b; 2015)).

Residuals were subsequently used to perform a series of two-block partial least squares analyses (2B-PLS; Rohlf & Corti, 2000; Zeldtich et al. 2004) to explore the covariation between pairs of bones from fore- and hind limbs. The comparisons were: humerus-femur, radius-tibia (both following a criterion of serial homology) and ulna-tibia. This comparison was made because the fibula (the serial homologous element of the ulna) is reduced in carnivorans, and it has been proposed that the tibia may have acquired some functions equivalent to those of the ulna (Martín-Serra et al. 2015). These analyses were also performed using MorphoJ (Klingenberg, 2011).

To specifically test if the associations between fore- and hind limbs of sabretooth predators are different to those of conical-tooth felids, we performed a series of bivariate regressions for the same bone comparisons (i.e., humerus-femur, radius-tibia, and ulna-tibia). We chose three proxies of limb strength: (*i*) the Log-transformed centroid sizes of the bones compared; (*ii*) their midshaft centroid sizes –calculated as the Log-transformed centroid sizes of the four landmarks describing the circumference at the middle of the diaphysis (see figure 1*b*); and (*iii*) their robustness –calculated as

198 the Log-transformed ratio of maximum bone length relative to midshaft diameter
199 (antero-posterior and medio-lateral average). The three measurements were calculated
200 using interlandmark distances (maximum length: landmarks 1-16 for the humerus, 4-9
201 for the radius, 1-18 for the ulna, 3-14 for the femur, and 4-22 for the tibia; for midshaft
202 landmarks, see figure 1*b*). It is worth noting that, throughout this article, we use the
203 words 'robust' or 'robustness' referring to bones that are relatively short and wide (i.e.,
204 stoutly-built), in contrast with others that are relatively long and narrow (i.e., gracile).
205 We use these differences in morphology as a proxy for limb strength. The
206 appropriateness of this approach is tested below.
207 For all bivariate regressions, we calculated the slopes for conical-tooth cats and
208 sabretooth forms independently using reduced major axis (RMA). This method is more
209 appropriate than ordinary least squares (OLS) to avoid the assumption that *y* depends on
210 *x* or *vice versa* (Quinn and Keough, 2002). Regression lines were derived using the
211 Paleontological Statistic Software (PAST; Hammer & Ryan, 2001). The slopes of sabre-
212 and conical-tooth forms were subsequently compared using a Student *t*-test (Sokal &
213 Rohlf, 1973).
214 In addition to the comparison of slopes, we also compared the regression
215 residuals of both conical- and sabretooth taxa to check if the forelimb bones of the latter
216 group are larger and/or more robust than those of their hind limb compared with the
217 relative size and/or robustness of the fore- and hind limbs of conical-tooth cats. The
218 main purpose of this additional comparison is to check if the differences between the
219 fore- and hind limb bones of sabretooths are due to a shift from the trend of conical-
220 tooth cats without changing their slope. Accordingly, given that we used conical-tooth
221 cats as a baseline for the association between the fore- and the hind limb, all the
222 residuals were extracted from the regression line of conical-tooth cats. For this purpose,

we calculated the residuals of conical-tooth cats using PAST and for sabretooth forms the residuals were calculated using the formula for Euclidean distance from a line to a point (Larson & Hostetler, 2007). As this formula yields absolute distance values, the negative or positive sign of each residual was assigned depending on its position with respect to the regression line in the plot.

The final step was to test if these morphological indices can be correctly interpreted as proxies for limb strength, as we are not measuring the cortical thickness of the bones. To do this, we used the external and internal diameters as well as the cortical areas of the humerus and femur in a number of living conical-tooth cats, the sabretooth *S. fatalis* and the extinct North American lion *Panthera atrox.* These data were retrieved from the database published by Meachen-Samuels and Van Valkenburgh (2010). We estimated the external and internal (medullary) surfaces of these bones using the average of their craniocaudal and mediolateral diameters at the diaphyseal midshaft. Then we plotted separately for the humerus and femur the log-transformed values of the internal diameter on the external diameter and computed OLS regressions. Finally, we log-log regressed for these species the cortical area of the femur on the cortical area of the humerus.

Results

Independent contrast analyses for the Procrustes coordinates on the Log-transformed centroid size (Log-Cs) were significant for all bone comparisons (table S5). Accordingly, we performed the 2B-PLS analyses using the residuals extracted from these regressions.

The 2B-PLS analyses showed that the first PLS axis of each analysis explained >70% of shape covariance in the three comparisons: 74.03% for humerus-femur, 94.31% for radius-tibia, and 97.07% for ulna-tibia. Bone robustness accounts for the

morphological changes associated with these first PLS axes (figure 2). From a visual inspection of these plots, we can observe that although most sabretooths plot within the morphological range of conical-tooth cats, some of them have extremely robust fore- and hind limb bones. However, even these forms seem to follow the same trend of conical-tooth cats.

The bone-to-bone bivariate regressions performed for conical and sabretooth forms with the three variables used (i.e., bone size, midshaft Cs and robustness index) yielded significant results in almost all cases (either at the 0.05 or 0.01 levels; see table 2). The only exception was the regression of robustness in sabretooths for the humerus-femur comparison (table 2), probably due to the small sample size. Therefore, the comparison of slopes with the *t*-test was not performed for this case. Among the remaining regressions, the slope test yielded non-significant results in most cases, which indicated the absence of differences between conical- and sabretooth predators in the pattern of correlation between the robustness of the fore- and the hind limb. There are three exceptions: (*i*) the regressions of centroid sizes between the humerus and femur (table 2), probably because *Megantereon cultridens* (6) and *Smilodon fatalis* (15) both have a larger humerus with respect to the femur than conical-tooth cats (figure 3*a*); (*ii*) the regressions of centroid sizes between the ulna and tibia (table 2), because *Hoplophoneus primaevus* (19) is an outlier with a tibia much larger than its ulna compared with conical-tooth cats (figure 3*c*), so it shifts the slope down (when this outlier is removed the slope test provides a non-significant result, $t = 0.243$, $p = 0.813$); and (*iii*) the regressions of the robustness indices between the radius and tibia (table 2), because, the increase of robustness in the tibiae of sabretooths is higher than the increase of robustness in their radii compared to conical-tooth cats (figure 3*h*). The graphical output of the calculated regression residuals (figure 4) confirms these results,

as sabretooths are placed in most cases within the range of conical-tooth cats or show a comparatively larger and/or more robust hind limb than its corresponding forelimb (e.g., figure 4*h*).

The regressions of the log-transformed values of the internal (medullary) area (*Y*-axis) on the external area (*X*-axis) at diaphyseal midshaft for the humerus and femur (species means obtained from data in Meachen-Samuels and Van Valkenburgh, 2010) are shown in figures 5*a*,*b* respectively. These regressions show that there is a statistically significant relationship between the external and internal measurements in both the humerus and the femur. Given that the cortical area of these limb bones is calculated as the difference between their external and medullary surfaces, this result indicates that the external diameters of the humerus and femur are good proxies of cortical thickness in felids. However, the slopes of these regressions (0.914 and 0.871, respectively) are lower than one, the expectation from isometric scaling, in both cases ($t_{hum} = 2.388$, $p < 0.02$; $t_{fem} = 3.085$, $p < 0.01$). This negative allometry indicates that the largest-sized felids have relatively smaller medullary areas in both major limb bones, which results in a more thickened cortical area (CA) for withstanding a greater weight.

In the case of the log-log regression of the CA values of the femur (*Y*-axis) on the CA values of the humerus (*X*-axis) (figure 5*c*), the departure of the slope (0.908) from isometric scaling is also statistically significant ($t = 2.04$, $p < 0.03$). This negative allometry indicates that the humerus is more stoutly built than the femur in the largest species, which probably reflects the need of a greater safety factor for the forelimb than for the hind limb in the largest felids. The reason is that the hind limb functions primarily in weight bearing and propulsion, whereas the forelimb is involved in a more varied repertory of functional tasks that require greater strength, including weight bearing, grasping the trunk and pulling the body upwards during climbing, prey

grappling and prey killing (Meachen-Samuels and Van Valkenburgh, 2009; Martín-Serra et al., 2015). In any case, the sabretooth *S. fatalis* lies within the 95% confidence interval of the regression line, which indicates that its humerus is scaled to the femur as in other felids, having the cortical thickness expected for a felid this large.

Discussion

The results obtained from the PLS analyses show that the morphological covariation of the fore- and the hind limb bones in sabre- and conical-tooth predators follow the same trend (figure 2). This suggests that the pattern of integration between the fore- and the hind limb bones of sabretooths is similar to the one depicted by conical-tooth cats. This is particularly striking, given that some sabretooth forms have extremely robust forelimb (and also hind limb) bones compared with those of conical-tooth cats (e.g., the genus *Smilodon* (15, 16); see figure 2*a*, *b*, *c*).

However, the absence of a different relationship between the fore- and the hind limbs in sabre- and conical-tooth predators was confirmed by a set of bivariate regressions (see figures 3 and 4). In fact, the size, midshaft Cs and robustness of the fore- and hind limb bones of sabretooths follow the same correlation pattern as in conical-tooth cats. With the only exception of the humerus-femur comparison, the regressions between the centroid sizes for the radius-tibia and ulna-tibia comparisons (figures 3*a*-*c*, 4*a*-*c*) show that the forelimb bones of sabretooths are not significantly larger than the bones of their hind limbs. The bone-to-bone regressions of the midshaft Cs (a proxy for bone resistance to bending stresses) indicate also that the midshaft circumference area of the fore- and hind limb bones increases in parallel for both conical- and sabretooth predators (figures 3*d*-*f*, 4*d*-*f*). Finally, the bone-to-bone regressions (figures 3*g*-*i*, 4*g*-*i*) of relative robustness indicate that the hind limb bones of

sabretooths are not less robust than their forelimb bones; indeed, it seems that some species are near the opposite situation (i.e., more robust hind limb bones than forelimb ones relative to conical-tooth cats; see, for example, figure 4*h*). Because stress resistance relies more on mid-shaft circumference area than on total bone size (Wroe et al. 2008), the fact that the humerus of sabretooths is larger than their femur does not seem to be a key feature for the hypothesis tested here. However, it could influence other aspects, such as the posture of the animal.

Although the small sample size for sabretooth forms must be taken into account regarding the significance of regression comparisons, an absence of a clear difference in the distribution of residuals for conical- and sabretooth forms indicates similar morphological patterns.

Following our results, the predatory specialization of sabretooth predators does not seem to involve a decoupled evolution of their fore- and hind limbs. The extremely strong forelimbs of some sabretooth forms such as *S. fatalis,* which were probably well adapted for prey immobilization (Gonyea, 1976; Antón et al. 2004; Christiansen, 2008; Salesa et al. 2010; Meachen-Samuels, 2012), are accompanied by extremely strong hind limbs, as inferred from the size and robustness of their bones.

It is worth remembering, however, that the phylogenetic corrections performed to discard the effects of evolutionary allometry reduce the phylogenetic signal to its lowest. This may also explain in part the absence of a difference in the scaling of the fore- and hind limbs between conical- and sabretooth predators once size was removed.

The only caveat that could be argued against our findings is that we have not measured bone cortical thickness, which is closely related to resistance to bending stress and, consequently, to limb strength (Anyonge, 1993, 1996; Meachen-Samuels and Van Valkenburgh, 2010). However, we have found a tight relationship between the external

and internal (medullary) areas of the humerus and femur in felids (figures 5*a*,*b*). Given that bone cortical thickness measures the difference between the external and medullary areas, this means that the external diameters of the humerus and femur are good proxies of their cortical thickness. However, as these slopes differ from one –i.e., the expectation of isometric scaling, largest species also have larger cortical areas. Moreover, the results shown in figure 5*c* clearly demonstrate that there is a tight relationship between the cortical area of the femur and humerus in felids and that the sabretooth *S. fatalis* is similarly scaled to other felids, although this relationship is again negatively allometric. This suggests that the cortical thickness of the humerus increases relative to that of the femur with body mass, which probably results from the greater demands of strength for the forelimb of felids, and *S. fatalis* was not an exception to this trend.

In any case, the slight dispersion around the regression line could be important to explore more subtle differences, such as those outlined by Meachen-Samuels and Van Valkenburgh (2010), who found that the humerus of *S. fatalis* was more resistant to bending stress along the mediolateral and craniocaudal planes than in other large felids except *P. atrox.* Meachen-Samuels and Van Valkenburgh (2010) regressed the indexes of bending stress of the humerus about the mediolateral and craniocaudal planes as well as its average rigidity in non-axial loading on the length of this bone, which showed that *S. fatalis* is an outlier to the trend of felids (Meachen-Samuels and Van Valkenburgh, 2010: figures 1*a*,*b*,*c*). However, it should be noted that the humerus is shorter in *S. fatalis* than in *P. atrox,* the largest conical-tooth cat of their sample, while both species show similar values of cortical area. This indicates that the greater resistance to bone stress of the humerus of *S. fatalis* was achieved by decreasing its length rather than increasing its cortical thickness, which also happened –but to a lesser extent– in the case

of the femur. Therefore, it seems that the specialization to the sabretooth predatory behaviour includes a great amount of parallel morphological changes in both limbs to increase their strength, which according to the scaling of these bones in felids resulted in slightly greater changes in the cortical area of their humerus with respect to their femur.

Conclusions

The results obtained in this study indicate that the predatory specialization of sabretooth predators does not involve a decoupled morphological evolution of their fore- and hind limbs, at least if they are compared with those of the living conical-tooth cats.

Therefore, this is a noteworthy case in which an adaptive process that modified intensely the morphology of both limbs was unable to alter the pattern of integration between them, probably due to the constraint posed by a strongly integrated developmental pattern. At first sight, this result seems to be in contrast with a previous study that demonstrated a shift towards a stronger pattern of between-limbs integration in specialized cursorial carnivorans (Martín-Serra et al. 2015). However, this can be due to different constraints depending on the direction of change (i.e., to increase the level of integration between the fore- and the hind limbs may be easier than to reduce it).

In any case, there is an alternative explanation for our results: maybe the presence of both strong fore- and hind limbs were adaptive for different reasons in sabretooth predators (e.g., the forelimbs helped in immobilizing prey and the hind limbs were useful for stabilizing the predator while subduing it). In such a case, the preserved pattern of integration between the fore- and the hind limbs could not result from the existence of strong developmental constraints but from parallel selective pressures.

Further studies on phenotypic integration at the intraspecific level will be very useful to uncover the mechanism that underlies this pattern.

Acknowledgements

We are especially grateful to F. Serrano for their comments and suggestions during the elaboration of this paper. We are also grateful to S. Almécija for providing us the bone scanning surfaces. We thank J. Galkin and E. Westwig (AMNH, New York), R. Portela and A. Currant (NHM, London), J. Morales and M. J. Salesa (MNCN, Madrid), L. Costeur (NMB, Basel), E. Cioppi (MSN, Firenze) and K. L. Hansen (SNM, Copenhagen) for kindly providing us access to the specimens under their care. This paper has been funded by the Spanish Ministry of Education PhD Research Fellowship (FPU: AP2008-00800) to AMS and the Spanish Ministry of Economy and Competitiveness (MINECO) grants of PP (CGL2008-04896 and CGL2016-78577-P) and BF (CGL2012-37866 and CGL2015-68300-P).

Author contributions

AMS collected the data and performed the analyses. AMS, BF and PP designed the study and wrote the manuscript. Neither author has any conflict of interest to declare.

References

Akersten WA (1985) Canine function in Smilodon (Mammalia: Felidae: Machairodontidae). Contrib Sci Nat Hist Mus Los Angeles County **356**, 1–22.

Andersson K, Norman D, Werdelin L (2011) Sabretoothed carnivores and the killing of large prey. PLoS ONE 6, e24971.

421 Anton M, Salesa MJ, Pastor JF, et al. (2004) Implications of the mastoid anatomy of
422 larger extant felids for the evolution and predatory behaviour of sabretoothed cats
423 (Mammalia, Carnivora, Felidae). Zool J Linn Soc **140**, 207–221.
424 Anyonge W (1993) Body mass in large extant and extinct carnivores. J Zool 231, 339–
425 350.
426 Anyonge W (1996) Locomotor behaviour in Plio- Pleistocene sabre-tooth cats: A
427 biomechanical analysis. J Zool **238**, 395–413.
428 Arribas A, Palmqvist P (1999) On the ecological connection between sabre-tooths and
429 hominids: faunal dispersal events in the lower Pleistocene and a review of the evidence
430 for the first human arrival in Europe. J Archaeol Sci **26**, 571–585.
431 Bell E, Andres B, Goswami A (2011) Integration and dissociation of limb elements in
432 flying vertebrates: a comparison of pterosaurs, birds and bats. J Evol Biol **24**, 2586–
433 2599.
434 Bertram JEA, Biewener AA (1990) Differential scaling of the long bones in the
435 terrestrial Carnivora and other mammals. J Morph **204**, 157–169.
436 Biknevicius AR, Van Valkenburgh B, Walker J (1996) Incisor size and shape:
437 implications for feeding behaviors in saber-toothed “cats”. J Vertebr Paleontol **16**, 510–
438 521.
439 Christiansen P (2008) Evolution of skull and mandible shape in cats (Carnivora:
440 Felidae). PLoS ONE **3**, e2807.
441 Christiansen P, Harris JM (2005) Body size of *Smilodon* (Mammalia: Felidae). J
442 Morphol **266**, 369–384.
443 Drake AG, Klingenberg CP (2008) The pace of morphological change: historical
444 transformation of skull shape in St Bernard dogs. Proc R Soc Lond B Biol Sci **275**, 71–
445 76.

446 Dryden IL, Mardia K (1998) Statistical Analysis of Shape. Chichester: Wiley.
447 Emerson SB, Radinsky L (1980) Functional analysis of sabertooth cranial morphology.
448 Paleobiology **6**, 295–312.
449 Figueirido B, MacLeod N, Krieger J, et al. (2011) Constraint and adaptation in the
450 evolution of carnivoran skull shape. Paleobiology **37**, 490–518.
451 Figueirido B, Tseng ZJ, Martín-Serra A (2013) Skull shape evolution in durophagous
452 carnivorans. Evolution **67**, 1975–1993.
453 Gonyea WJ (1976) Behavioral implications of saber-toothed felid morphology.
454 Paleobiology **2**, 332–342.
455 Goswami A, Weisbecker V, Sánchez-Villagra MR (2009) Developmental modularity
456 and the marsupial-placental dichotomy. J Exp Zool **312**, 186–195.
457 Goswami A, Polly PD, Mock OB, et al. (2012) Shape, variance and integration during
458 craniogenesis: contrasting marsupial and placental mammals. J Evol Biol **25**, 862–872.
459 Hallgrímsson B, Willmore K, Hall BK (2002) Canalization, developmental stability,
460 and morphological integration in primate limbs. Am J Phys Anthropol **45**, 131–158.
461 Hallgrímsson B, Jamniczky H, Young NM, et al. (2009) Deciphering the palimpsest:
462 studying the relationship between morphological integration and phenotypic
463 covariation. Evol Biol **36**, 355–376.
464 Hammer ØHD, Ryan PD (2001) PAST: Paleontological statistics software package for
465 education and data analysis. Palaeontol Electronica **4**, 9.
466 Klingenberg CP (2008) Morphological integration and developmental modularity. Ann
467 Rev Ecol Evol Syst **39**, 115–132.
468 Klingenberg CP (2011) MorphoJ: an integrated software package for geometric
469 morphometrics. Mol Ecol Res **11**, 353–357.

Klingenberg CP, Marugán-Lobón J (2013) Evolutionary covariation in geometric morphometric data: analyzing integration, modularity, and allometry in a phylogenetic context. Syst Biol **62**, 591–610.

Larson R, Hostetler RP (2007) Precalculus: a concise course. Boston: Houghton Mifflin.

Lewis ME, Lague MR (2010) Interpreting sabertooth cat (Carnivora; Felidae; Machairodontinae) postcranial morphology in light of scaling patterns in felids. In: *Carnivoran evolution: new views on phylogeny, form and function.* (eds. Goswami A, Friscia A), pp. 411–465, Cambridge: Cambridge University Press.

Maddison WP, Maddison DR (2011) Mesquite: a modular system for evolutionary analysis. Version 2.75. Available via http://mesquiteproject.org.

Martin LD (1980) Functional morphology and the evolution of cats. Trans Nebr Acad Sci **8**, 141–154.

Martín-Serra A, Figueirido B, Palmqvist P (2014a) A three-dimensional analysis of morphological evolution and locomotor performance of the carnivoran forelimb. PloS ONE **9**, e85574.

Martín-Serra A, Figueirido B, Palmqvist P (2014b) A three-dimensional analysis of the morphological evolution and locomotor behaviour of the carnivoran hind limb. BMC Evol Biol **14**, 129.

Martín-Serra A, Figueirido B, Pérez-Claros JA, et al. (2015) Patterns of morphological integration in the appendicular skeleton of mammalian carnivores. Evolution **69**, 321–340.

McHenry C, Wroe S, Clausen PD, et al. (2007) Supermodeled sabercat, predatory behavior in *Smilodon fatalis* revealed by high-resolution 3D computer simulation. Proc Nat Acad Sci USA **104**, 16010–16015.

495 Meachen-Samuels JA (2012) Morphological convergence of the prey-killing arsenal of
496 sabertooth predators. Paleobiology **38**, 715–728.
497 Meachen-Samuels JA, Van Valkenburgh B (2009) Forelimb indicators of prey-size
498 preference in the Felidae. J Morphol **270**, 729–744.
499 Meachen-Samuels JA, Van Valkenburgh B (2010) Radiographs reveal exceptional
500 forelimb strength in the sabertooth cat, *Smilodon fatalis*. PLoS ONE **5**, e11412.
501 Monteiro LR (1999) Multivariate regression models and geometric morphometrics: the
502 search for causal factors in the analysis of shape. Syst Biol **48**, 192–199.
503 Monteiro LR, Nogueira MR (2010) Adaptive radiations, ecological specialization, and
504 the evolutionary integration of complex morphological structures. Evolution **64**, 724–
505 744.
506 Nyakatura K, Bininda-Emonds ORP (2012) Updating the evolutionary history of
507 Carnivora (Mammalia): a new species-level supertree complete with divergence time
508 estimates. BMC Biol **10**, 12.
509 Palmqvist P, Torregrosa V, Pérez-Claros JA, et al. (2007) A re-evaluation of the
510 diversity of *Megantereon* (Mammalia, Carnivora, Machairodontinae) and the problem
511 of species identification in extinct carnivores. J Vert Paleontol **27**,160–175.
512 Quinn GP, Keough MJ (2002) Experimental design and data analysis for biologists.
513 Cambridge: Cambridge University Press.
514 Rohlf FJ, Corti M (2000) Use of two-block partial least-squares to study covariation in
515 shape. Syst Biol **49**, 740–753.
516 Salesa MJ, Antón M, Turner A, et al. (2010) Functional anatomy of the forelimb in
517 *Promegantereon ogygia* (Felidae, Machairodontinae, Smilodontini) from the Late
518 Miocene of Spain and the origins of the saber-toothed felid model. J Anat **216**, 381–
519 396.

Singleton M (2012) Postnatal cranial development in papionin primates: An alternative model for hominin evolutionary development. Evol Biol **39**, 499–520.

Slater GJ, Van Valkenburgh B (2008) Long in the tooth: evolution of sabertooth cat cranial shape. Paleobiology **34**, 403–419.

Sokal RR, Rohlf FJ (1973) Introduction to Biostatistics. (2nd ed.). San Francisco: WH Freeman and Co.

Van Valkenburgh B (2001) Predation in sabre-tooth cats. Pp. 420–423 in D. E. G. Briggs and P. R. Crowther, eds. Paleobiology II. Blackwell

Van Valkenburgh B (2007) De´ ja` vu: the evolution of feeding morphologies in the Carnivora. Integrative and Comparative Biology 47:147–163.

Wagner GP, Altenberg L (1996) Complex adaptations and the evolution of evolvability. Evolution **50**, 967–976.

Wagner GP, Pavlicev M, Cheverud J (2007) The road to modularity. Nat Genet **8**, 921–931.

Wiley DF, Amenta N, Alcantara DA, et al. (2005) Evolutionary Morphing. In: *Proceedings of IEEE Visualization 2005 (VIS'05)*, pp. 431–438.

Wilson T, Wilson DE, Zimanske JM (2013) Pneumothorax as a predatory goal for the sabertooth cat (*Smilodon fatalis*). Open J Anim Sci 3, 42–45.

Wroe S, Lowry MB, Anton M (2008) How to build a mammalian super-predator. Zool **111**, 196–203.

Young NM, Hallgrímsson B (2005) Serial homology and the evolution of mammalian limb covariation structure. Evolution **59**, 2691–2704.

Young RL, Badyaev AV (2006) Evolutionary persistence of phenotypic integration: influence of developmental and functional relationships on complex trait evolution. Evolution **60**, 1291–1299.

545 Zelditch ML, Swiderski DL, Sheets HD, et al. (2004) Geometric morphometrics for
546 biologists: a primer. San Diego: Elsevier.
547

Table and figure captions

Table 1. List of species and number of specimens for each bone analysed in this study. H, humerus; R, radius; U, ulna; F, femur; T, tibia. Daggers denote extinct species.

Family	Species (code number)	H	R	U	F	T
Barbourofelidae	*Barbourofelis fricki* (1) †	0	3	0	0	2
Felidae	*Acinonyx jubatus* (2)	5	5	5	5	5
	Leptailurus serval (3)	2	2	2	2	2
	Lynx rufus (4)	4	4	4	4	4
	Machairodus aphanistus (5) †	0	2	3	0	1
	Megantereon cultridens (6) †	2	3	2	1	1
	Neofelis nebulosa (7)	1	1	1	1	1
	Panthera leo (8)	5	5	5	5	5
	Panthera onca (9)	4	4	4	4	4
	Panthera pardus (10)	6	6	6	6	6
	Panthera tigris (11)	4	4	4	4	4
	Promegantereon ogygia (12) †	3	5	2	4	2
	Pseudaelurus (13) †	1	3	0	1	2
	Puma concolor (14)	4	4	4	4	4
	Smilodon fatalis (15) †	1	1	1	1	1
	Smilodon populator (16) †	0	1	1	0	1
	Uncia uncia (17)	4	4	4	4	4
Nimravidae	*Dinictis* (18) †	3	0	0	5	0
	Hoplophoneus primaevus (19) †	0	2	1	0	1
	Pogonodon (20) †	0	1	0	0	2

Table 2. Results obtained in the bone-to-bone bivariate regressions. All relevant regression parameters are shown for each comparison, including the coefficient of determination (R^2), the slope of RMA, the standard error (SE) and the number of cases (n). Student t-tests, their degrees of freedom (Df) and the P-value for the comparisons between the slopes of the two groups are also shown. HF, humerus-femur; RT, radius-tibia; UT, ulna-tibia. Significance: 0.01 (**), 0.05 (*).

		Conical-tooth cats				Sabretooth predators				Student *t*-test		
		r^2	Slope	SE	n	r^2	Slope	SE	n	t	df	P-value
Centroid size	**HF**	0.986**	1.007	0.04	11	0.988*	0.835	0.065	4	2.263*	11	0.045
	RT	0.95**	0.858	0.064	11	0.878**	0.757	0.108	8	0.8	15	0.436
	UT	0.971**	0.868	0.053	10	0.862**	0.577	0.107	6	2.432*	12	0.032
Midshfat Cs	**HF**	0.968**	0.821	0.049	11	0.994*	0.704	0.039	4	0.239	11	0.816
	RT	0.937**	0.785	0.065	11	0.865**	0.713	0.107	8	0.576	15	0.573
	UT	0.829**	0.866	0.127	10	0.777*	0.512	0.121	6	2.027	12	0.065
Robustness	**HF**	0.757**	0.448	0.074	11	0.755	0.504	0.176	4			
	RT	0.674**	0.506	0.096	11	0.884**	1.171	0.162	8	-3.516**	15	0.003
	UT	0.506*	0.483	0.12	10	0.717*	0.715	0.19	6	-1.0324	12	0.322

588 **Figure 1**. Phylogeny and morphometrics. (*a*) Assembled phylogenetic tree, including
589 the relative branch lengths and time scale (My) used in this study (see text for details);
590 (*b*) three-dimensional landmarks located on the limb bones analysed.
591
592 **Figure 2.** Bivariate graphs for the first PLS axes obtained from the comparisons
593 between limb bones. Percentages of covariance explained by PLS axes shown: 74.03%,
594 94.31%, and 97.07% for (a), (b) and (c) respectively. Equal frequency ellipses at 95% of
595 probability are also shown (red for conical-tooth cats and blue for sabretooth forms).
596 Bone models show the morphological variation accounted for by each axis. For species
597 code numbers, see table 1.
598
599 **Figure 3.** Bivariate regressions for bone-to-bone comparisons. Regressions with total
600 centroid size (*a*-*c*), midshaft Cs (*d*-*f*) and robustness index (*g*-*i*). RMA regression lines
601 for conical-tooth cats (red) and sabretooth predators (blue) are shown. For species code
602 numbers, see table 1; for group colours, see figure 2.
603
604 **Figure 4.** Univariate plots of the residuals obtained from the bone-to-bone RMA
605 regressions for conical-tooth cats. Residuals for total centroid size (*a*-*c*), midshaft Cs (*d*-
606 *f*) and robustness index (*g*-*i*). The horizontal dashed line indicates the RMA regression
607 line for conical-tooth cats. For species code numbers, see table 1; for group colours, see
608 figure 2.
609
610 **Figure 5.** Least-squares regressions of log-transformed values of external area on
611 internal (medullary) area measured at diaphyseal midshaft for the humerus (A) and
612 femur (B) in a sample of living felids plus the extinct sabretooth *S. fatalis* and giant lion

P. atrox. C: Log-log regression of femur cortical area (CA) on humerus CA. Dashed lines represent the 95% intervals above and below the regression line. Ajub: *Acinonyx jubatus,* Ccar: *Caracal caracal,* Cser: *Caracal serval,* Lcan: *Lynx canadensis,* Lruf: *Lynx rufus,* Lpar: *Leopardus pardalis,* Patr: *Panthera atrox* (†), Pben: *Prionailurus bengalensis,* Pcon: *Puma concolor,* Pmar: *Pardofelis marmorata,* Pleo: *Panthera leo,* Ponc: *Panthera onca,* Ppar: *Panthera pardus,* Ptig: *Panthera tigris,* Punc: *Panthera uncia,* Pyag: *Puma yagouroundi,* Sfat: *Smilodon fatalis* (†). Means for felid species obtained from data in Meachen-Samuels & Van Valkenburgh (2010).

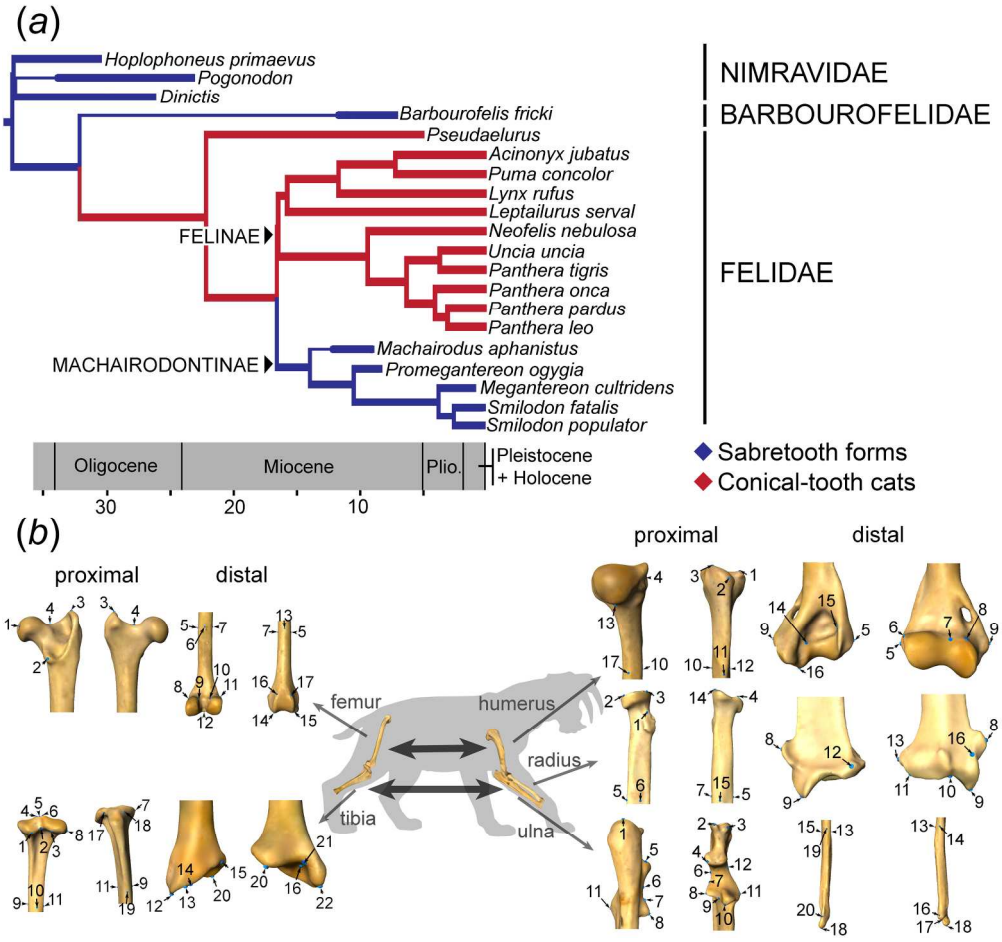

Figure 1. Phylogeny and morphometrics. (a) assembled phylogenetic tree, including the relative branch lengths and time scale (My) used in this study (see text for details); (b) three-dimensional landmarks located on the limb bones analysed.

107x101mm (600 x 600 DPI)

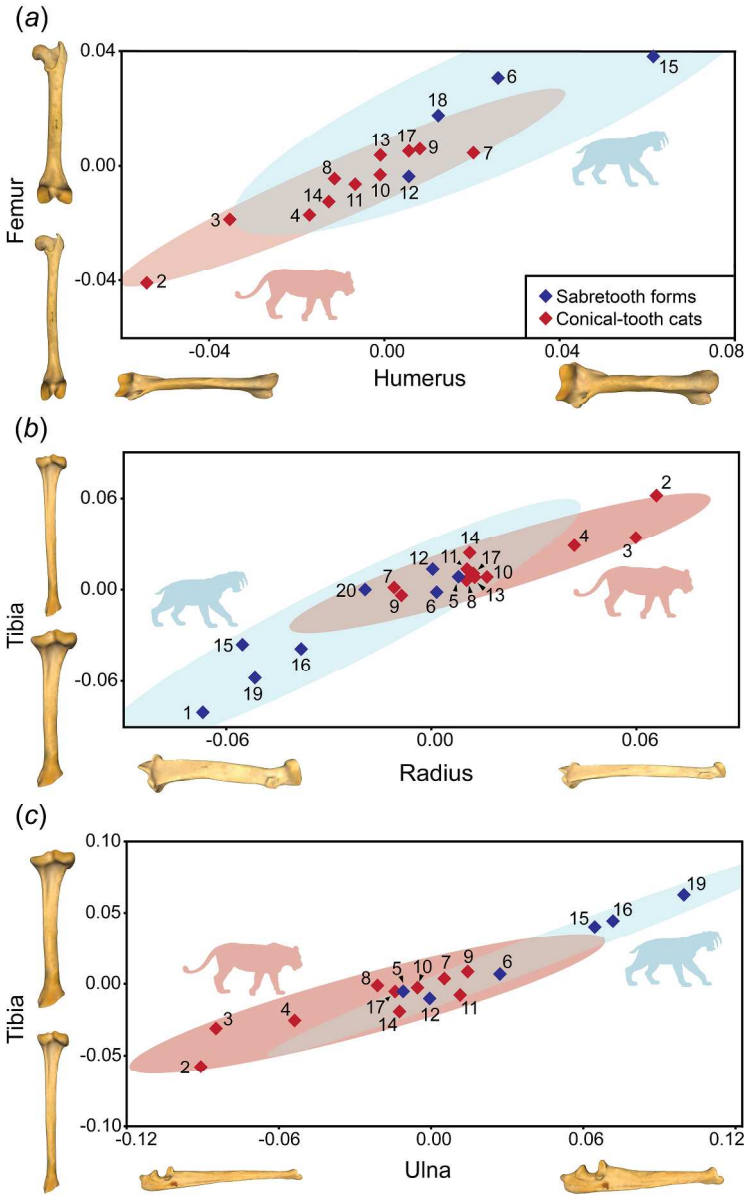

Figure 2. Bivariate graphs for the first PLS axes obtained from the comparisons between limb bones. Percentages of covariance explained by PLS axes shown: 74.03%, 94.31%, and 97.07% for (a), (b) and (c) respectively. Equal frequency ellipses at 95% of probability are also shown (red for conical-tooth cats and blue for sabretooth forms). Bone models show the morphological variation accounted for by each axis. For species code numbers, see table 1.

185x301mm (300 x 300 DPI)

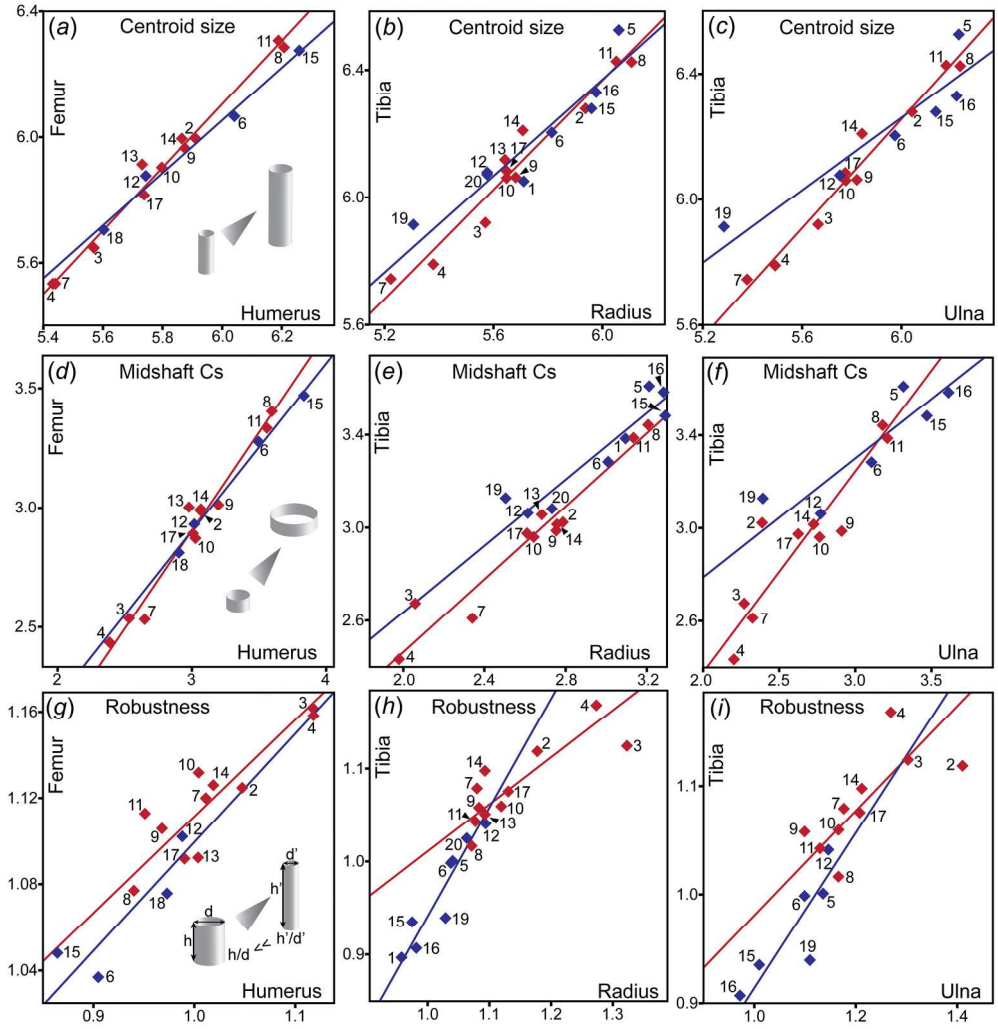

Figure 3. Bivariate regressions for bone-to-bone comparisons. Regressions with total centroid size (a-c), midshaft Cs (d-f) and robustness index (g-i). RMA regression lines for conical-tooth cats (red) and sabretooth predators (blue) are shown. For species code numbers, see table 1; for group colours, see figure 2.

184x191mm (300 x 300 DPI)

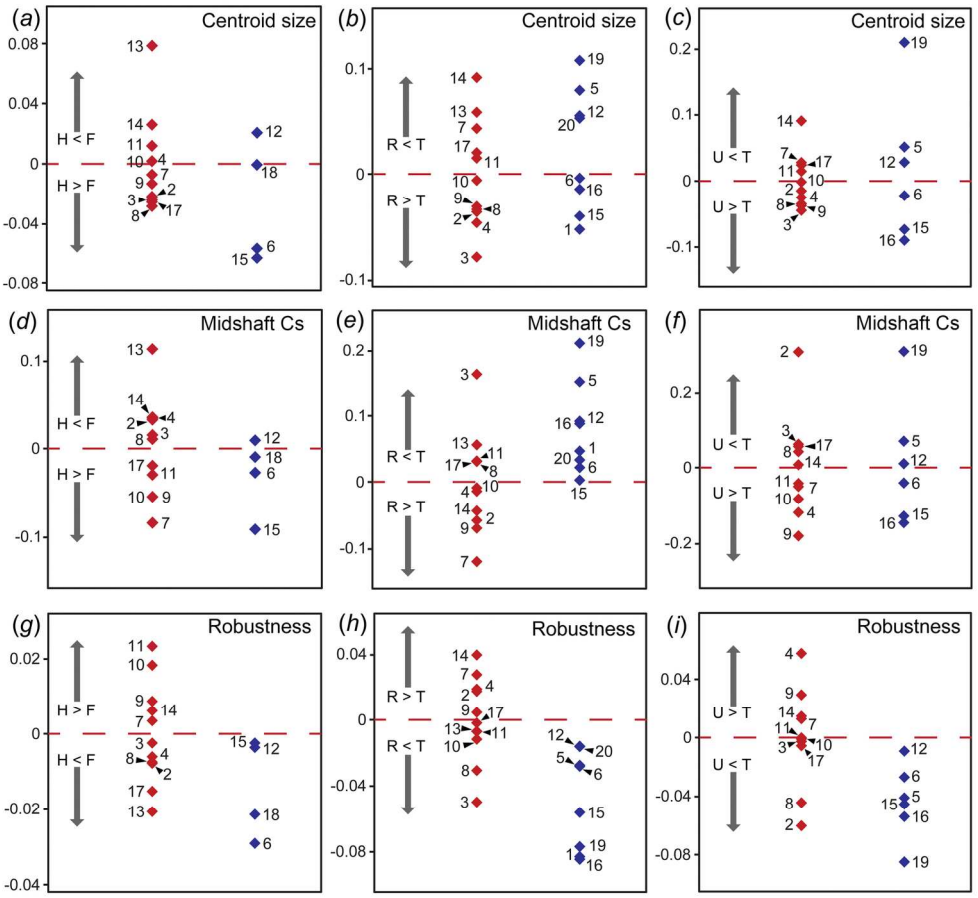

Figure 4. Univariate plots of the residuals obtained from the bone-to-bone RMA regressions for conical-tooth cats. Residuals for total centroid size (a-c), midshaft Cs (d-f) and robustness index (g-i). The horizontal dashed line indicates the RMA regression line for conical-tooth cats. For species code numbers, see table 1; for group colours, see figure 2.

164x150mm (300 x 300 DPI)

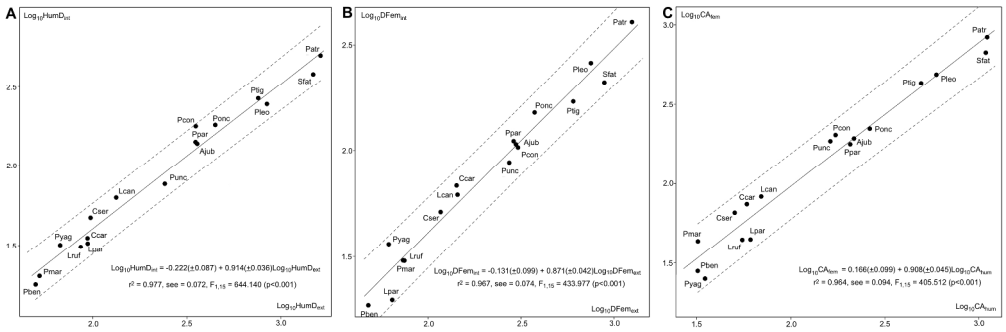

Figure 5. Least-squares regressions of log-transformed values of external area on internal (medullary) area measured at diaphyseal midshaft for the humerus (A) and femur (B) in a sample of living felids plus the extinct sabretooth S. fatalis and giant lion P. atrox. C: Log-log regression of femur cortical area (CA) on humerus CA. Dashed lines represent the 95% intervals above and below the regression line. Ajub: Acinonyx jubatus, Ccar: Caracal caracal, Cser: Caracal serval, Lcan: Lynx canadensis, Lruf: Lynx rufus, Lpar: Leopardus pardalis, Patr: Panthera atrox (†), Pben: Prionailurus bengalensis, Pcon: Puma concolor, Pmar: Pardofelis marmorata, Pleo: Panthera leo, Ponc: Panthera onca, Ppar: Panthera pardus, Ptig: Panthera tigris, Punc: Panthera uncia, Pyag: Puma yagouroundi, Sfat: Smilodon fatalis (†). Means for felid species obtained from data in Meachen-Samuels & Van Valkenburgh (2010).

1121x366mm (72 x 72 DPI)

Table S1. List of specimens of living species included in the analyses. Identity number (ID) and hosting institution are also shown. AMNH, American Museum of Natural History (New York, USA); NHM, Natural History Museum (London, UK).

Species	ID	Host Institution
Acinonyx jubatus	119654	AMNH
Acinonyx jubatus	119655	AMNH
Acinonyx jubatus	119656	AMNH
Acinonyx jubatus	1940.1.20.17	NHM
Acinonyx jubatus	1962.7.6.15	NHM
Leptailurus serval	119207	AMNH
Leptailurus serval	27837	AMNH
Lynx rufus	119206	AMNH
Lynx rufus	208417	AMNH
Lynx rufus	128527	AMNH
Lynx rufus	171361	AMNH
Neofelis nebulosa	238650	AMNH
Panthera leo	1952.10.20.13	NHM
Panthera leo	112.a	NHM
Panthera leo	1857.2.24.1	NHM
Panthera leo	75.1998	NHM
Panthera leo	75.945	NHM
Panthera onca	35571	AMNH
Panthera onca	139959	AMNH
Panthera onca	135928	AMNH
Panthera onca	1858.5.26.9	NHM
Panthera pardus	209087	AMNH
Panthera pardus	1940.1.20.18	NHM
Panthera pardus	115p	NHM
Panthera pardus	1851.2.17.3	NHM
Panthera pardus	1940.1.20.20	NHM
Panthera pardus	1849.6.20.2	NHM
Panthera tigris	113743	AMNH
Panthera tigris	113748	AMNH
Panthera tigris	135846	AMNH
Panthera tigris	85404	AMNH
Puma concolor	1335	AMNH
Puma concolor	90213	AMNH
Puma concolor	14026	AMNH
Puma concolor	135341	AMNH
Uncia uncia	207704	AMNH
Uncia uncia	266952	AMNH
Uncia uncia	119662	AMNH
Uncia uncia	100110	AMNH

Table S2. List of specimens of extinct species included in the analyses. Identity number (ID) and hosting institution are also shown. AMNH, American Museum of Natural History (New York, USA); NMB, Naturhistorisches Museum Basel (Switzerland); MNCN, Museo Nacional de Ciencias Naturales (Madrid, Spain); SNM, Staten Naturhistoriske Museum (Copenhagen, Denmark).

Species	ID	Host Institution
Humerus		
Dinictis sp.	125652 L	AMNH
Dinictis sp.	125652 R	AMNH
Dinictis sp.	1396	AMNH
Megantereon cultridens	Se311 L	NMB
Megantereon cultridens	Se311 R	NMB
Promegantereon ogygia	B-2465	MNCN
Promegantereon ogygia	BAT-1-'03-D4-361	MNCN
Promegantereon ogygia	BAT-3-'08-70	MNCN
Pseudaelurus sp.	62202	AMNH
Smilodon fatalis	LB41	NMB
Radius		
Barbourofelis fricki	2672	AMNH
Barbourofelis fricki	61998	AMNH
Barbourofelis fricki	61999	AMNH
Hoplophoneus primaevus	655	AMNH
Hoplophoneus primaevus	38980	AMNH
Machairodus aphanistus	B-1482	MNCN
Machairodus aphanistus	B-2621	MNCN
Megantereon cultridens	Se311	NMB
Megantereon cultridens	StV774.1953	NMB
Megantereon cultridens	VA1201	NMB
Pogonodon sp.	1399	AMNH
Promegantereon ogygia	B-2207A	MNCN
Promegantereon ogygia	B-4413	MNCN
Promegantereon ogygia	B-4566	MNCN
Promegantereon ogygia	BAT-1-'05-D8-30	MNCN
Promegantereon ogygia	BAT-3-9-'01	MNCN
Pseudaelurus sp.	61942-A	AMNH
Pseudaelurus sp.	62209	AMNH
Pseudaelurus sp.	62225	AMNH
Smilodon fatalis	LB41	NMB
Smilodon populator	1.7.85-2	SNM
Ulna		
Hoplophoneus primaevus	38980	AMNH
Machairodus aphanistus	B-2365	MNCN
Machairodus aphanistus	B-2624	MNCN

Machairodus aphanistus	B-2720	MNCN
Megantereon cultridens	Se311	NMB
Megantereon cultridens	VA1201	NMB
Promegantereon ogygia	BAT-1-'02-E7-72	MNCN
Promegantereon ogygia	BAT-3-5-38	MNCN
Smilodon fatalis	LB41	NMB
Smilodon populator	2	SNM
Femur		
Dinictis sp.	125652	AMNH
Dinictis sp.	62074	AMNH
Dinictis sp.	62122	AMNH
Dinictis sp.	69425	AMNH
Dinictis sp.	69426	AMNH
Megantereon cultridens	Se311	NMB
Promegantereon ogygia	B-3-2561	MNCN
Promegantereon ogygia	BAT-1-'01-D6-115	MNCN
Promegantereon ogygia	BAT-1-'08-D3-4	MNCN
Promegantereon ogygia	BAT-1-'08-E3-26	MNCN
Pseudaelurus sp.	62167	AMNH
Smilodon fatalis	LB41	NMB
Tibia		
Barbourofelis fricki	61994	AMNH
Barbourofelis fricki	61995	AMNH
Hoplophoneus primaevus	655	AMNH
Machairodus aphanistus	B-398	MNCN
Megantereon cultridens	Se311	NMB
Pogonodon sp.	1399 L	AMNH
Pogonodon sp.	1399 R	AMNH
Promegantereon ogygia	BAT-1-'05-F6-42	MNCN
Promegantereon ogygia	BAT-1-'06-F4-232	MNCN
Pseudaelurus sp.	62163	AMNH
Pseudaelurus sp.	62173	AMNH
Smilodon fatalis	LB41	NMB
Smilodon populator	2	SNM

Table S3. Detailed description of the anatomical position of each landmark used in this study.

	Humerus:
1	Most proximal point of the lesser tuberosity.
2	Most proximal point of the greater tuberosity.
3	Most anterior point of the greater tuberosity.
4	Midpoint of the infraspinatus insertion fossa.
5	Most lateral point of the lateral epicondyle.
6	Lateral-proximal corner of the capitulum at the anterior side.
7	Point of maximum curvature of the articular surface at the anterior side of its proximal border.
8	Medial-proximal corner of the trochlea at the anterior side.
9	Most medial point of the medial epicondyle.
10	Most lateral point at the middle of the shaft.
11	Most anterior point at the middle of the shaft.
12	Most medial point at the middle of the shaft.
13	Most distal point of the humeral head.
14	Medial-proximal corner of the trochlea at the posterior side
15	Lateral-proximal corner of the capitulum at the posterior side.
16	Most distal point of the trochlear ridge.
17	Most posterior point at the middle of the shaft.
	Radius:
1	Most proximal point of the bicipital tuberosity.
2	Point of maximum curvature of the head border of the radius at the medial side.
3	Point of maximum curvature of the head border of the radius at the posterior side.
4	Most proximal point in the radial coronoid process.
5	Most medial point at the middle of the shaft.
6	Most posterior point at the middle of the shaft.
7	Most lateral point at the middle of the shaft.
8	Most medial point of the distal epiphysis.
9	Most distal point of the radial styloid process.
10	Most proximal point of the anterior border of the distal articular surface.
11	Most lateral point of the anterior border of the distal articular surface.
12	Most posterior point of the distal epiphysis.
13	Most lateral point of the distal epiphysis.
14	Point of maximum curvature of the radius head border at the lateral side.
15	Most anterior point at the middle of the shaft.
16	Most proximal point of the radial styloid process at the anterior side.

	Ulna:
1	Most proximal point of the olecranon process.
2	Most anterior point of the lateral edge of the olecranon process.
3	Most anterior point of the medial edge of the olecranon process.
4	Most anterior point of the anconeus process.
5	Most distal point of the trochlear groove at the lateral side.
6	Midpoint of the lateral border of the trochelar groove.
7	Point of maximum curvature between the border of the trochlear groove and the beginning of the lateral coronoid process.
8	Most lateral point of the lateral coronoid process.
9	Midpoint of the distal border of the radial groove.
10	Most anterior point of the medial coronoid process.
11	Most medial point of the trochlear groove border.
12	Point of maximum curvature of the medial border of the trochlear groove, where the anconeus process begins.
13	Most lateral point at the middle of the shaft.
14	Most anterior point at the middle of the shaft.
15	Most medial point at the middle of the shaft.
16	Most anterior point of the distal epiphysis.
17	Point of maximum curvature at the beginning of the ulnar styloid process.
18	Most distal point of the ulnar styloid process.
19	Most posterior point at the middle of the shaft.
20	Most posterior point of the distal epiphysis.

	Femur:
1	Midpoint of the fovea capitis.
2	Most posterior point of the lesser trochanter.
3	Most proximal point of the greater trochanter.
4	Point of maximum curvature in the proximal edge between the femoral head and the greater trochanter.
5	Most medial point at the middle of the shaft.
6	Most posterior point at the middle of the shaft.
7	Most lateral point at the middle of the shaft.
8	Proximo-medial corner of the medial condyle.
9	Proximo-lateral corner of the medial condyle.
10	Proximo-medial corner of the lateral condyle.
11	Proximo-lateral corner of the lateral condyle.
12	Most distal point of the intercondylar fossa.
13	Most anterior point at the middle of the shaft.
14	Point of maximum curvature of the lateral edge between the condyle and the trochlea.
15	Point of maximum curvature of the medial edge between the condyle and the trochlea.
16	Most proximal point of the lateral edge of the trochlea.
17	Most proximal point of the medial edge of the trochlea.

	Tibia:
1	Point of maximum curvature of the posterior edge of the medial condyle.
2	Point of maximum curvature of the posterior intercondylar edge.
3	Point of maximum curvature of the posterior edge of the lateral condyle.
4	Most proximal point of the medial condyle.
5	Point of maximum curvature in the intercondylar eminence.
6	Most proximal point of the lateral condyle.
7	Most medial point of the proximal epiphysis.
8	Most lateral point of the proximal epiphysis.
9	Most medial point at the middle of the shaft.
10	Most posterior point at the middle of the shaft.
11	Most lateral point at the middle of the shaft.
12	Postero-distal corner of the medial malleolus.
13	Most distal point of the posterior edge of the distal articular surface.
14	Most posterior point of the internal edge of the distal articular surface.
15	Most proximal point of the lateral edge of the distal articular surface.
16	Midpoint of the medial half of the distal articular surface.
17	Point of maximum curvature of the lateral edge of the tibial tuberosity.
18	Point of maximum curvature of the medial edge of the tibial tuberosity.
19	Most anterior point at the middle of the shaft.
20	Most distal point of the anterior edge of the distal articular surface.
21	Point of maximum curvature in the notch of the anterior edge of the distal articular surface.
22	Antero-distal corner of the medial malleolus.

Table S4. Stratigraphic ranges and time of divergence for the extinct taxa included in the composite tree used in this paper. The source references for phylogenetic position and stratigraphic range are indicated.

Taxa	Stratigraphic range	Ref. for phylogenetic position	Ref. for stratigraphic range
Barbourofelis fricki	12.1 - 7 my	Morlo et al. 2004	Tseng et al. 2010
Dinictis	35.1 - 30.4 my	Peigné 2003	Martin 1998, Peigné 2003, Janis et al. 2008
Hoplophoneus primaevus	35.5 - 30.4 my	Peigné 2003	Martin 1998, Peigné 2003, Janis et al. 2008
Machairodus aphanistus	12.5 - 9 my	Anton et al. 2004	Werdelin and Peigne 2010
Megantereon cultridens	3.6 - 0.78 my	Anton et al. 2004	Palmqvist et al. 2007
Pogonodon	34 - 23 my	Peigné 2003	Peigné 2003, Martin 1998, Janis et al. 2008
Promegantereon ogygia	10.3 - 8.2 my	Salesa et al. 2010	NOW database
Pseudaelurus	22 - 4.9 my	Rothwell 2003	FossilWorks
Smilodon fatalis	2.4 - 0.01 my	Werdelin et al. 2010	Werdelin et al. 2010
Smilodon populator	2.3 - 0.01 my	Werdelin et al. 2010	Werdelin et al. 2010
	Time of divergence		**Ref. for time of divergence**
Family Barbourofelidae	32 my	Morlo et al. 2004	Werdelin et al. 2010
Family Nimravidae	37 my	Peigné 2003	Martin 1998, Peigné 2003, Janis et al. 2008
Subfamily Machairondontinae	14 my	Werdelin et al. 2010	Werdelin et al. 2010

Anton M, Salesa MJ, Morales J, Turner A. 2004 First known complete skulls of the scimitar-toothed cat *Machairodus aphanistus* (Felidae, Carnivora) from the Spanish late Miocene site of Batallones-1. *J. Vertebr. Paleontol.* **24**, 957–968.

Fortelius M. (coordinator) 2015 New and Old Worlds Database of Fossil Mammals (NOW). University of Helsinki. http://www.helsinki.fi/science/now/.

Janis CM, Gunnell G, Uhen M. 2008 Evolution of Tertiary Mammals of North America Vol. 2: Small Mammals, Edentates, and Marine Mammals. Cambridge, UK: Cambridge University Press. 802 p.

Martin LD. 1998 Nimravidae. In *Evolution of Tertiary mammals of North America: Volume 1, terrestrial carnivores, ungulates, and ungulate like mammals* (eds Janis CM, Scott KM, Jacobs LL), pp: 228–235. Cambridge: Cambridge University Press.

Morlo M, Peigne S, Nagel D. 2004 A new species of *Sansanosmilus*: implications for the systematic relationships of the family Barbourofelidae new rank (Carnivora, Mammalia). *Zool. J. Linn. Soc.* **140**, 43–61.

Palmqvist P, Torregrosa V, Pérez-Claros JA, Martínez-Navarro B, Turner A. 2007 A re-evaluation of the diversity of *Megantereon* (Mammalia, Carnivora, Machairodontinae) and the problem of species identification in extinct carnivores. *J. Vertebr. Paleontol.* **27**, 160–175.

Peigné S. 2003 Systematic review of European Nimravinae (Mammalia, Carnivora, Nimravidae) and the phylogenetic relationships of Palaeogene Nimravidae. *Zool. Scr.* **32**, 199–229.
Rothwell T. 2003 Phylogenetic systematics of Northamerican *Pseudaelurus* (Carnivora, Felidae). *Am. Mus. Nov.* **3403**, 64.
Salesa MJ, Antón M, Turner A, Morales J. 2010 Functional anatomy of the forelimb in *Promegantereon ogygia* (Felidae, Machairodontinae, Smilodontini) from the Late Miocene of Spain and the origins of the sabre-toothed felid model. *J. Anat.* **216**, 381–396.
Tseng ZJ, Takeuchi GT, Wang X. 2010 Discovery of the upper dentition of *Barbourofelis whitfordi* (Nimravidae, Carnivora) and an evaluation of the genus in California. *J. Vertebr. Paleontol.* **30**, 244–254.
Werdelin L, Peigné S. 2010 Carnivora. In *Cenozoic Mammals of Africa* (eds Werdelin L, Sanders WJ), pp. 609–663. Berkeley: University of California Press.
Werdelin L, Yamaguchi N, Johnson WE, O'Brien SJ. 2010 Phylogeny and evolution of cats (Felidae). In *Biology and conservation of wild felids* (eds Macdonald DW, Loveridge AJ), pp. 59–82. Oxford, UK: Oxford University Press.

Table S5. Results obtained from the preliminary analyses of phylogenetic signal and evolutionary allometry for each bone. For the phylogenetic signal analyses, tree lengths and p values (between brackets) are shown. For the multivariate regressions between the contrasts of shape and the contrasts of size, percentage of variance explained and p value (between brackets) are shown.

BONE	Ind. cont. shape	Reg. shape-size
Humerus	0.0184 (0.003)	34.10% (0.0003)
Radius	0.024 (0.0011)	11.91% (0.0501)
Ulna	0.0352 (0.0132)	31.71% (0.0003)
Femur	0.0102 (0.0015)	23.83% (0.0013)
Tibia	0.0194 (0.0058)	18.93% (0.0073)